Program Digest, 2019 IEEE International Ultrasonics Symposium (IUS)
Glasgow, Scotland, October 6-9, 2019

Full Wave 3D Inverse Scattering Transmission Ultrasound Tomography: Breast and Whole Body Imaging

James Wiskin, PhD, MSc
Principal Scientist
QT Ultrasound, LLC
Novato, CA, USA
james.wiskin@qtultrasound.com

Bilal Malik, PhD, MSc
Principal Scientist
QT Ultrasound, LLC
Novato, CA, USA
bilal.malik@qtultrasound.com

Rajni Natesan, MD, MBA
CMO
QT Ultrasound, LLC
Novato, CA, USA
rajni.natesan@qtultrasound.com

David Borup, PhD
Principal Scientist
QT Ultrasound, LLC
Novato, CA, USA
david.borup@qtultrasound.com

Nasser Pirshafiey, MBA
CPO
QT Ultrasound, LLC
Novato, CA, USA
nasser.pirshafiey@qtultrasound.com

Mark Lenox
Dept of Bioengineering
Texas A&M Univ.
College Station, TX, USA
markwlenox@tamu.edu

John Klock
CEO *, Managing Director*
QT Ultrasound, LLC
Novato, CA, USA
john.klock@qtultrasound.com

***Abstract*—Encouraged by progress over the past 10 years in breast imaging, we have generalized 3D ultrasound transmission tomography (UST) to orthopaedic, whole body and clinical applications. We document quantitative breast density measurement, quantitative transmission tomography in the presence of bone and air, and tumor monitoring applications, indicating that 3D UST is a whole body imaging modality with clinical implications.**

Keywords*—3D transmission ultrasound tomography, refraction corrected reflection, inverse scattering, quantitative transmission ultrasound, breast density, orthopaedic, whole-body imaging, tumor monitoring.

I. Introduction

Beginning with early work by Greenleaf and Johnson at the Mayo Clinic in 1974-1980, ultrasound tomography (UST) has developed into a useful modality for breast imaging. Original work by Johnson's group at the University of Utah led to high contrast and spatial resolution images in 2008, which were steadily improved at QT Ultrasound, resulting in FDA clearance for a clinical grade scanner in 2017.

Extensive research has also been carried out by groups in Karlsruhe, Netherlands, Michigan, USA, and elsewhere[1-7]. There has been crossover interest from several groups in Geophysical imaging [8-12]. Clinical breast data is now being acquired throughout the US and analyzed.

In this paper we will concentrate on the tomographic system being developed presently by QT Ultrasound Labs[13-15].

Tomographic systems generally utilize either ray based techniques[16], which do not incorporate diffraction effects, wave based inverse scattering techniques, which incorporate all wave phenomena, or a hybrid method for the transmission mode tomography. e.g. see [17]. Our approach is in effect a coefficient determination problem for partial differential equations (PDE) and thus computationally expensive.

To make the method practical, we use frequency domain data, and utilize a parabolic (paraxial) approximation to the full Helmholtz equation[18]. This yields a very fast forward problem solver, concomitant Jacobian, and the required fast implementation of the adjoint of the Jacobian calculation, after some algebraic manipulation. See [13] and below, for details.

This is similar to the phase screen approach common in optics, oceanography, etc. which is based on an approximate factorization of the Helmholtz equation[19].

Our initial success in breast imaging and related protocols has led to our objective of extending UST to the more difficult scenario of whole body and orthopedic imaging, where bone and air are present, and to the translation of the high resolution speed and reflection images into clinically useful metrics such as quantitative breast density (QBD) assessment, and quantitative tumor monitoring (QTM).

We have generalized the reconstruction protocols used for breast imaging to achieve high resolution, speed of sound and reflection images of the whole body. We have quantitatively imaged soft tissue that does not generate an MR signal, near mature bone, and in the whole body of neo-natal piglets.

Note that the quantitative imaging of bone itself is not the goal of this paper. This is believed to require additional modelling involving shear and possibly Biot waves.

A. Quantitative speed of sound measurement.

We wish to quantitatively image -- to high resolution -- muscle, cartilage, tendons, ligaments, nerve bundle tissue, veins even in the presence of bone and air.

Requiring quantitative accuracy is related to minimizing the 'volume averaging effect', wherein adjacent pixel values are smeared together, thereby affecting the accuracy of all relevant voxels. Thus high resolution is paramount.

B. 360-degree compounded refraction corrected reflection image

Refraction corrected reflection imaging has been carried out by several research groups and is an ongoing area of study [16]. Our success with the breast imaging paradigm and related protocols leads to the desire to test this algorithm in the more difficult scenario where bone and air are present. Also, this imaging procedure is important in the removal of clutter (see below) and determination of breast density (QBD).

C. Tumor volume measurement for QTM:

We also desire quantitative and accurate volumetric estimation of tumor size. This is important in the monitoring of cancer treatments. It is important in testing clinical protocols that the efficacy of the treatment is adjudicated quickly and accurately.

When cancerous lesions do not respond to treatment it is important to change to a new treatment as quickly as possible, so that the correct treatment is found. Our reflection and transmission algorithms provide the means for high resolution segmentation of the relevant tumor. Thus volumetric changes can be accurately seen very quickly into a treatment program, without contrast agents or ionizing radiation.

D. QBD

It is recognized that Tyrer-Cuzick and other models of risk require an estimate of breast density in their calculations.

For this and other reasons, it is important to be able to measure the breast density accurately.

II. Statement of Contribution/Methods

A. Contribution

We have

- generalized the reconstruction protocols used for breast imaging to achieve high resolution, speed of sound and reflection images of the whole body in presence of bone and air. .
- quantitatively imaged cartilage, tendons, ligaments and other soft tissue near mature bone, (some of which do not generate an MR signal), and
- imaged structure/tissue in the whole body of neo-natal piglets.
- developed quantitative methods for the assessment of breast tissue fibroglandular volume, i.e. breast density (QBD), and
- developed a protocol for quantitative tumour monitoring (QTM)

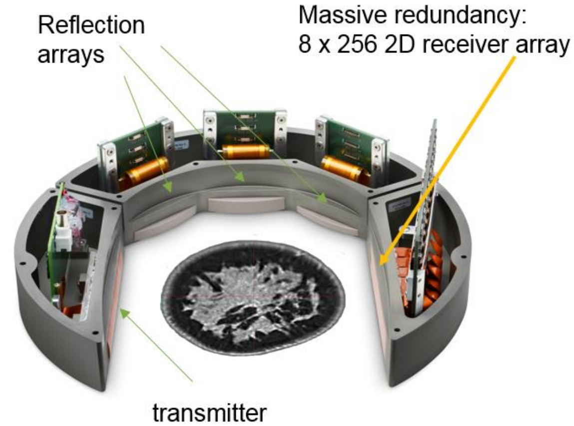

Fig. 1. QT Ultrasound Scanner (top panel) and arrays (bottom panel)

B. Methods

1) Data acquisition

The ultrasound scanner consists of a plane wave transmitter, a 2048 element receiver array, and 3 adjunct reflection arrays in a water bath. The arrays rotate completely (tomographically) around the object in the water bath, shooting an acoustic wave that interacts with the object according to the Helmholtz equation, then is received on the opposite side. The 2048 array elements are arranged in a rectangular geometry and receive the transmitted waveforms after they have passed through the subject., Waveform measurements are individually Fourier transformed to discrete frequencies, which are successively used in the frequency domain fully 3D inverse scattering algorithm that incorporates the 3D nature of the acoustic field. The entire apparatus is moved upward approximately 2 mm and another rotation carried out. Simultaneously, reflection data is collected from the 3 arrays discussed in [15, 20] to be used in a concomitant refraction corrected (3D) reflection algorithm that incorporates the speed of sound (SOS) map generated by the inverse scattering reconstruction.

2) Processing – Quantitative inverse scattering model

We use a model based large scale minimization based on an L_2 norm cost function. We minimize over a representation, γ of the speed of sound and attenuation of the object at each voxel. The data residual is defined as the difference between the predicted $\hat{\mathbf{d}}^{l}_{\omega_j\theta}$ and measured $\mathbf{d}^{l}_{\omega_j\theta}$ data

$$\mathbf{r}^{l}_{\omega_j\theta} \equiv \left(\hat{\mathbf{d}}^{l}_{\omega_j\theta} - \mathbf{d}^{l}_{\omega_j\theta}\right) \in \mathbf{C}^{N_R} \qquad (1)$$

Where the vector **r** encapsulates the difference at each vertical level *l, and* azimuthal angle θ, for a particular frequency ω_j. The total L_2 over all views (angles), levels and elements is minimized at each frequency. That is, we minimize the L_2 norm of this residual vector over all views: all levels and azimuthal angles, and over successive frequencies.

We start at low frequencies, i.e. at 0.3 MHz, and move progressively upward in variable increments (approximately .1 MHz) until we stop at ~ 1.3 MHz, thereby avoiding local minima as the low frequency data yields low resolution images. The algorithm successively adds higher frequency information to the known good image and continues to the high frequency – high resolution image. The particular frequency and iteration selection varies with the particular case, and scenario (breast, whole body, orthopaedic, extremity etc.):

- Breast imaging
- Orthopaedic/extremity imaging
- Knee
- Whole body (meso-body imaging)
- QBD assessment
- QTM (quantitative tissue monitoring)

The reflection data are utilized as time domain waveforms and backprojected as dictated by the ray-tracing algorithm based on the method of lines approach to the eikonal equation.

Since we are carrying out a large scale minimization, a nonlinear conjugate gradient based method is used (based on the Polyak-Ribiere-Polak beta coefficient for directional update). This requires the following:

3) Forward problem

The forward problem is solved via the paraxial approximation to the full Helmholtz equation. Thus, we solve a parabolic partial differential equation in place of the elliptic Helmholtz PDE, and accept associated errors in angle and approximate boundary conditions.

4) Jacobian formulation

The concomitant Jacobian is calculated analytically from the forward problem. This linear operator is calculated at the discrete level, thereby avoiding issues with discretization after the adjoint formulation. The Jacobian is calculated using a perturbation method and is the exact Jacobian calculation within the constraints of the aforementioned paraxial approximation and the discretization. Thus, it is, by definition, also a recursion operation and ideally suited to solve the minimization problem within the paraxial approximation. This is used in the step length estimation, and in the formulation of the adjoint.

5) Adjoint of the Jacobian

The adjoint of the Jacobian of the forward problem is determined within the paraxial approximation from the above Jacobian. Both of these linear operations are also recursions, and therefore much faster than trying to invert a large matrix, which would result if the Helmholtz equation itself were solved.

6) Paraxial approximation

The approximation is shown *a posteriori* to be accurate. We have compared the geometric distribution of speed of sound images of breasts, knees and whole piglets with MR images and found close agreement.

Note this is mathematically similar to the adjoint method employed in geophysics and oceanography, but the recursive nature of the paraxial approximation makes the numerical solution faster.

This last observation is critical to the deployment of the machine to a clinical setting

C. Refraction Corrected reflection image

The reflection image is formed by solving the set of ordinary differential equations (ODE's) which result from applying the method of lines to the nonlinear second order partial differential equation – the eikonal equation. This in turn arises from the asymptotic expansion of the solution to the Helmholtz equation. The resulting ray tracing algorithm is ubiquitous in geophysics, oceanography, medical imaging, and other large scale imaging problems.

The resulting reflection image can be compounded over a full 360 degrees due to the refraction correction step inherent in the solution of the system of ODE's. It is calibrated to be perfectly correlated with the SOS image.

1) Post-processing: declutter

After the inverse scattering procedure is carried out a decluttering algorithm is applied to the speed of sound and reflection images. This algorithm is related to the QBD algorithm.

The attenuation image is primarily utilized as a constraint within the declutter paradigm. An unsharp masking filter is applied to the refraction corrected reflection image to increase the resolution.

Quantitative Breast density (QBD)

We have several QBD algorithms. They are similar in their determination of the breast volume. However, they differ in their respective determination of the fibroglandular tissue as distinct from the rest of the breast. The algorithm shown here is based on a speed of sound segmentation. This has shown to be effective in volume determination[21].

The versions of the QBD algorithm that have been tested:

QBD algorithm with reflection and SOS/atten based segmentation.

QBD algorithm without reflection (uses SOS and attenuation only) and SOS/atten based segmentation.

QBD with FCM clustering algorithm

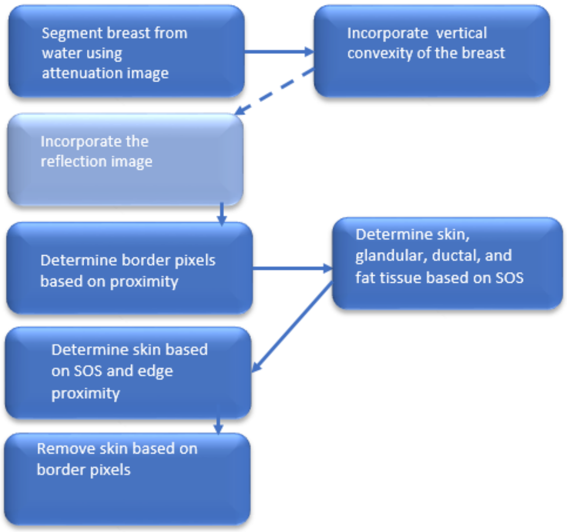

Fig. 2. An example representation of a QBD algorithm.

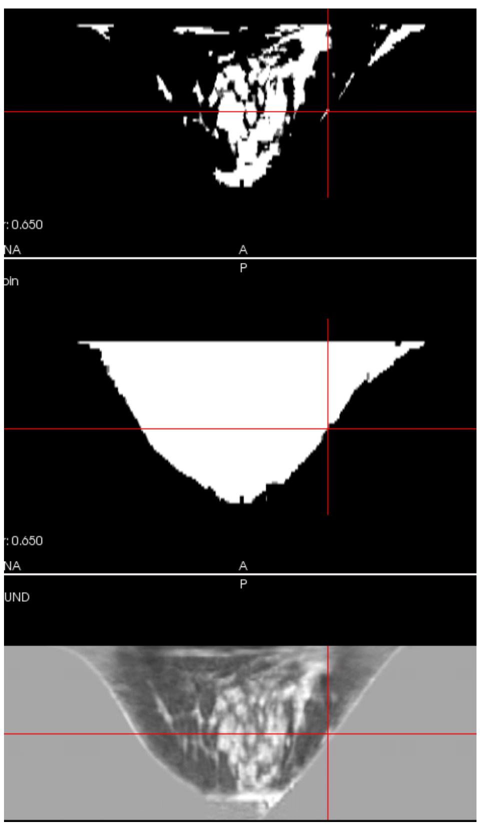

Fig. 3. Visual representation of QBD calculation. The top panel shows the segmented fibroglandular tissue without skin. Middle is breast volume w/o skin. Bottom is speed of sound original image. Axial view of the breast.

These QBD algorithms were used on 248 breasts to estimate breast density and correlated to measurements of breast density from Volpara™, an FDA approved method for breast density estimation from mammography.

D. Quantitative Tumor Monitoring (QTM)

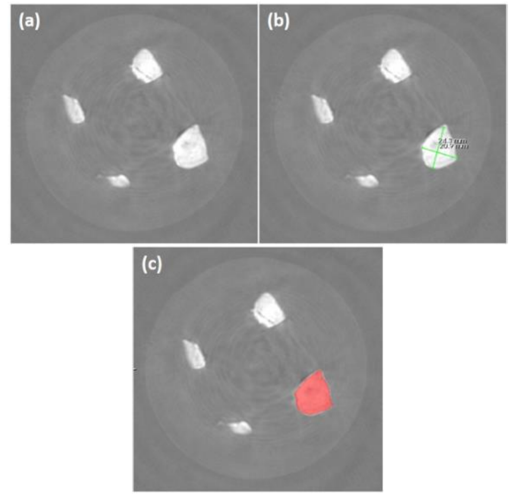

Fig. 4. Speed of sound transmission tomography images of (a) an agar phantom with embedded lesions, (b) a single lesion measured with calipers, (c) automated calculation of the lesion volume using a thresholded segmentation algorithm

For comparison 6 agar phantoms containing 4 'lesions' each, of chicken tissue, were constructed.(Fig. 4). These 24 lesions were visualized using Hand Held Ultrasound (HHUS) and measured in 3 dimensions (major axes: *a,b,c*) and volumes were calculated using 2 different formulas:

(1) sphere: $\frac{\pi}{6}d^3$ (*with d = 'diameter'* = average of *a, b, and c*)

(2) ellipsoid: $\frac{\pi}{6}abc$

The Ultrasound Tomography (UST) image volumes were calculated with automated segmentation software (QT Ultrasound, Novato, CA)

The Volumetric measurement accuracy of both UST and HHUS were compared to known true volumes calculated by the water displacement methods. Results discussed below.

E. Results/Discussion

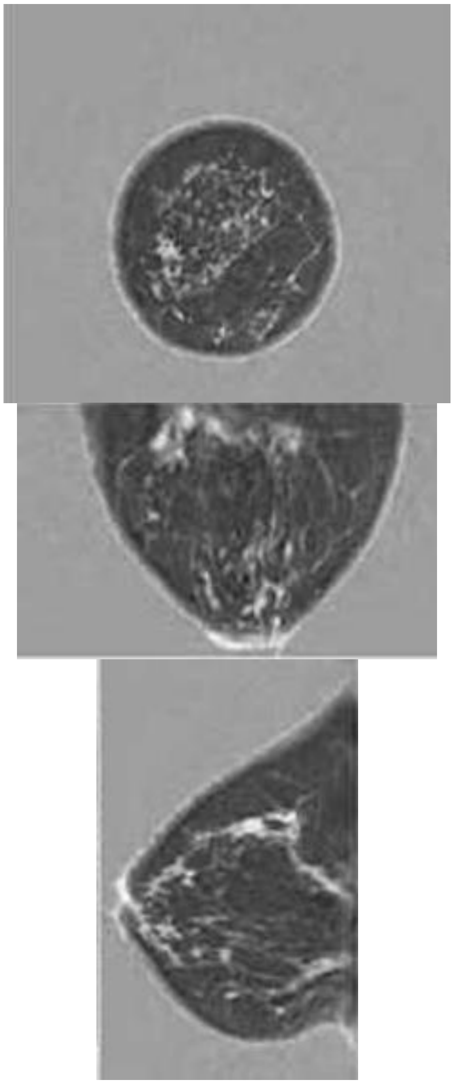

Fig. 5. : Top: coronal, middle axial and bottom : sagittal views of the transmission ultrasound 3D speed of sound map. This image shows clearly the 3D nature of the image created by the 3D transmission ultrasound algorithm using fully 3D data.

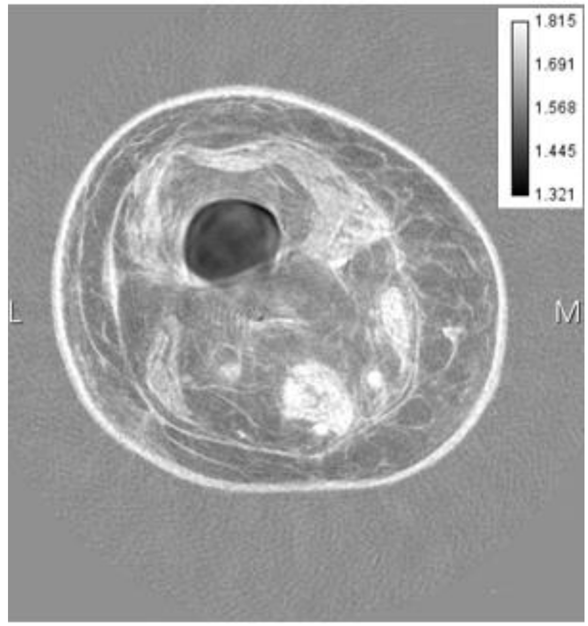

Fig. 6. : axial, view of fused SOS and reflection image of mature human knee above the tibio-femural space. This is standard grayscale showing the vastus lateralis, vastus medialis, biceps femoris, semimembranosus, and sartorius muscle. The high speed patellar tendon, the cartilage and biceps femoris muscle tendon complex show as light gray (high speed) lateral to femur. Detailed connective tissue structure is visible in the surrounding tissue. The femur has a very low (incorrect) speed of sound but the rest of the tissue is correctly reconstructed to high resolution.

Fig. 6 shows the capability of the algorithm to reconstruct quantitatively and at high resolution, the speed of sound of tissue surrounding the mature human knee.

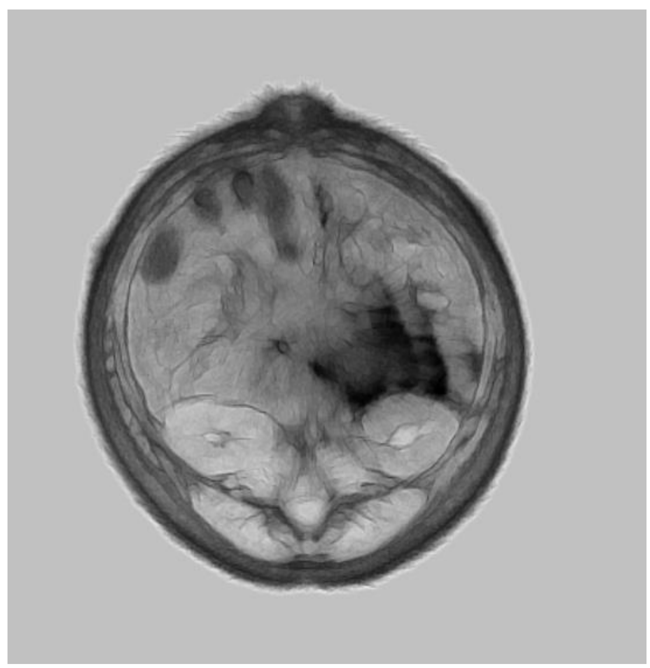

Fig. 7. Axial cross-section view of a fused speed of sound – reflection image of the neo-natal piglet. This is inverted grayscale showing the vertebral body, kidneys (renal medulla, and cortex, pelvis and ureter), epaxial and other muscles are clearly seen, the small intestine is visible in interior, and the spiral colon is visible in the center (dark gray scale)

1) QBD

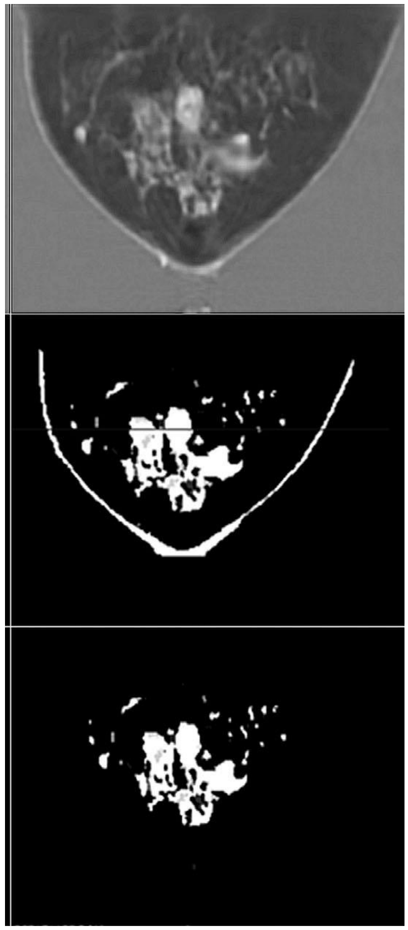

Fig. 8. : Steps in one of the QBD algorithms: Top row, speed-of-sound images. Middle row, breast separated from the water bath with skin and fibroglandular tissue segmented from the total breast tissue volume. Bottom row, remaining fibroglandular tissue following the segmentation and removal of skin. The segmentation is based on SOS > 1489 m/s.

Fig. 7 shows the axial view of the fused SOS and reflection images of a neo-natal piglet.

This shows the quantitative accuracy and stability of the reconstructions in the presence of bone and air, and contrast and spatial resolution of the SOS and reflection images.

Note that even in the presence of air the quantitative accuracy and high resolution is not greatly affected.

Fig. 8 shows the progression in one of our QBD algorithms for the determination of the fibroglandular tissue volume. The skin and fibroglandular tissue are isolated after the breast has been isolated using attenuation and convexity assumptions. Then the skin is removed using proximity relations. This serves as the numerator in the QBD calculation (see also Fig. 3)

2) Accuracy/Stability over time – reproducibility

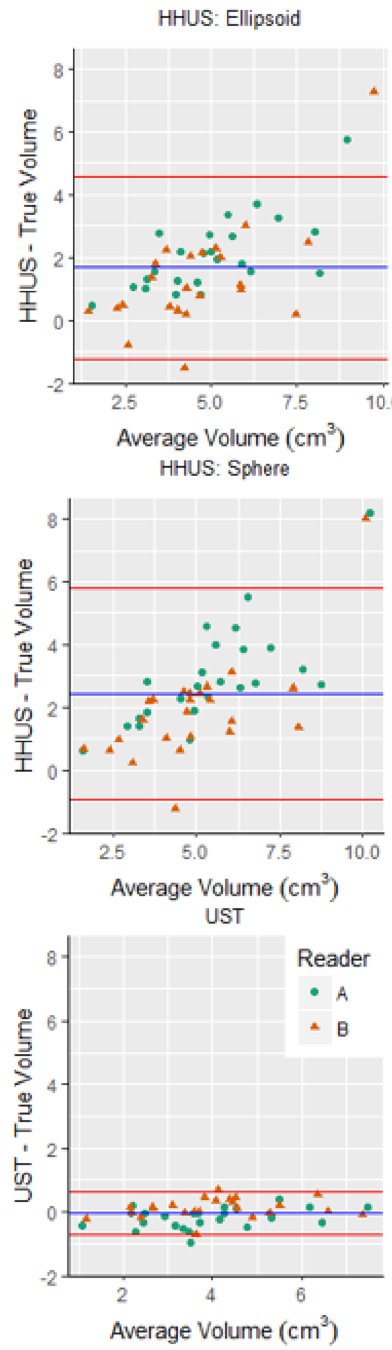

Fig. 9. The difference in volume measurements vs average volume : top : volume from HHUS minus true volume (ellipsoidal formula), middle : HHUS volume – True Volume, and bottom 3D UST Volume minus True volume vs average volume

We achieve quantitative accuracy of tissue in knee and piglet images, and complete femur/tibia separation with 'volumetric bone reconstruction' protocols in the case of the knee.

Cartilage and ligaments interior and close to the Femur-Tibia (F-T) space are imaged, even when corresponding MR images fail to show signal from tendons (such as biceps femoris, and patellar tendons).

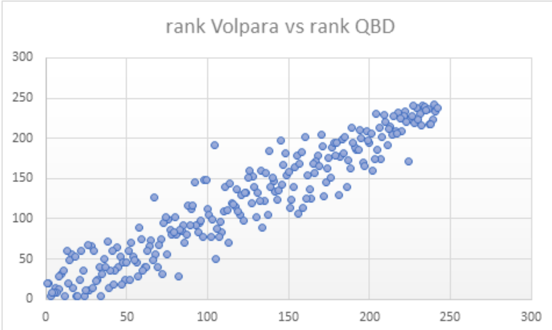

Fig. 10. Typical Scatter plot of rank from Volpara score vs rank from our QBD algorithm. The corresponding Spearman rank coefficient was 0.93.

This quantitative high-resolution accuracy is achieved even in the presence of mature, large bone (distal epiphysis of femur and proximal epiphysis of tibia).

The SOS and reflection fused image of the neo-natal piglet in Fig. 7, shows intestines, internal organs, kidneys, and vertebrae. to high resolution and accuracy in axial view.

Fig. 9 shows the estimates of the differences of volumes of the 24 lesions embedded in the 6 agar phantoms. Whether the ellipsoidal rule or the sphere rule formulas are used, the differences between the true volume and the UST volume are statistically significantly different from the differences between the HHUS measured and the true volumes, as is evident from this figure.

Fig. 10 shows correlation between the Volpara™ ranking and the QTUS based QBD ranking for 248 breasts. Implants were excluded in this plot. The Spearman rank coefficient was 0.93 for this data set based on the QBD utilizing reflection and SOS segmentation. The other algorithms gave similar results.

III. CONCLUSION :

Whole body, extremity and orthopaedic imaging:

Transmission ultrasound imaging has high spatial/contrast resolution and is safe for broadly applicable human medical imaging.

We have shown success already in breast imaging [15]. The a posteriori evidence of the quantitative accuracy and high resolution of our knee and whole body (piglet) images indicates the capability of our algorithm (paraxial approximation) to account for these high contrast media, and still give correct SOS, attenuation, and reflection values for surrounding tissue to high accuracy and resolution.

We note however, that the speed of sound of the bone itself is not reconstructed. This is to be expected since the acoustic penetration at the frequencies we employ will be small, due to the standoff distance between the transmitter and the bone.

The refraction corrected reflection image, compounded over 360 degrees yields high resolution images of connective tissue well correlated with the SOS map after calibration, and thus easily fused to it, as in Fig. 6, thereby yielding high resolution images of connective tissue.

The ability to quantitatively estimate in high resolution the speed of sound of muscle, cartilage, tendons, ligaments even in the presence of bone (note we do not claim to accurately measure the SOS of bone presently) means the capability to monitor strained ligaments/tendons that may be susceptible to breakage in horses, or humans in athletic endeavours, thereby preventing more serious damage.

The monitoring of cartilage also makes possible arthritic monitoring and diagnosis. Duchenne Muscular Dystrophy can also be monitored effectively and non-invasively without ionizing radiation. The imaging of meso-body images (neonates) allows the imaging of neo-nates without high magnetic fields or ionizing radiation.

QTM:

We can monitor the efficacy of cancer treatments relatively quickly due to the high accuracy and stability of the volume measurement of the lesions we observe. Furthermore, the imaging of the lesion can be easily and repeatedly carried out with transmission ultrasound, without radiation or contrast agents.

QBD:

Quick, accurate estimate of breast density (QBD), is a part of several risk assessment protocols (e.g. Tyrer-Cusick). We have shown a correlation with our QBD estimator and the FDA approved Volpara™ score. Thus the QTUS image and QBD algorithm is well suited for cancer risk assessment.

The speed of sound enables the speckle free high-resolution reflection image compounded over 360 degrees.

The efficacy of the imaging modality with limited views allows the use of a treatment on site that can be monitored in vivo by the imaging device. The limited view capability in conjunction with the capability in presence of bone and air allows the imaging and treatment of deep internal organs such as the prostate.

Not shown but important for understanding breast structure is the 3D printing capability derived from the QTUS images. Such 3D printing has revealed increased connectivity and unexpected flatness of the fibroglandular structure.

The timing of the image creation (breast – ½ hour, knee and meso-body : ~0.7 to 1.2 hours.) is reasonable but not ideal, from a clinical point of view.

There are certainly non-trivial engineering problems yet to be overcome, but we believe we have shown that the combination of full wave speed of sound transmission tomography and refraction corrected reflection imaging is poised to become a true whole body imaging modality.

This is especially true with the implementation of the paraxial approximation with the concomitant speed up and the highly redundant fully 3D data acquisition system

ACKNOWLEDGMENT

We gratefully acknowledge the laboratory work of Dr. V. Theendakara, Robin Terry, M. Sc. and the Clinical staff at QT Ultrasound, LLC, and QT Breasthealth™, support from TIPS

(Texas A&M Institute for Preclinical Studies) and Dr. C. Ruoff, DVM and support from NIH: NCI R01-CA138536

[1] N. V. Ruiter, M. Zapf, T. Hopp, R. Dapp, E. Kretzek, M. Birk, *et al.*, "3D ultrasound computer tomography of the breast: A new era?," *European Journal of Radiology,* vol. 81, pp. S133-S134, 2012.

[2] K. W. A. v. Dongen, L. Demi, and M. D. Verweij, "Numerical schemes for the Iterative Nonlinear Contrast Source method," *The Journal of the Acoustical Society of America,* vol. 132, pp. 1918-1918, 2012.

[3] N. D. Duric, C. Li, P. Littrup, L. Huang, C. K. Glide-Hurst, O. Ramsa, *et al.*, "Detection and characterization of breast masses with ultrasound tomography: clinical results," in *SPIE 72651G*, 2009, pp. 72651G_1, 72651G_8.

[4] M. Sak, N. Duric, P. Littrup, L. Bey-Knight, H. Ali, P. Vallieres, *et al.*, "Using Speed of Sound Imaging to Characterize Breast Density," *Ultrasound in Medicine & Biology,* vol. 43, pp. 91-103, 1// 2017.

[5] M. Andre, H. Janee, G. Otto, P. Martin, B. Spivey, and D. Palmer, "High speed data acquisition in a diffraction tomography system employing large-scale toroidal arrays," *Int. J. Imaging Syst. Technol.,* pp. 137-147, 1997.

[6] R. Lavarello and M. Oelze, "A Study on the Reconstruction of Moderate Contrast Targets Using the Distorted Born Iterative Method," *Trans. Ultrasonics, Ferroelectrics and Freq. Control,* vol. 55, pp. 112-124, 2007.

[7] R. J. Lavarello and M. Oelze, "Tomographic reconstruction of Three Dimensional volumes Using the Distorted Born Approximation," *IEEE Transactions on Medical Imaging,* vol. 28, pp. 1643-1653, 2009.

[8] R. G. Pratt, C. Shin, and G. J. Hick, "Gauss–Newton and full Newton methods in frequency–space seismic waveform inversion," *Geophysical Journal International,* vol. 133, pp. 341-362, 1998.

[9] N. Korta Martiartu, N. Vinard, C. Boehm, I. Jovanovic, and A. Fichtner, *Optimized transducer configuration for ultrasound waveform tomography in breast cancer detection*, 2018.

[10] A. TARANTOLA, "LINEARIZED INVERSION OF SEISMIC REFLECTION DATA*," *Geophysical Prospecting,* vol. 32, pp. 998-1015, 1984.

REFERENCES

[11] C. Li and N. Duric, "Resolution limitation of travel time tomography: beyond the first Fresnel zone," 2013, pp. 86751D-86751D-10.

[12] K. Wang, T. Matthews, F. Anis, C. Li, N. Duric, and M. A. Anastasio, "Waveform Inversion With Source Encoding for Breast Sound Speed Reconstruction in Ultrasound Computed Tomography," *IEEE Transactions on Ultrasonics, Ferroelectrics and Frequency Control,* vol. 62, pp. 475-493, 2015.

[13] J. Wiskin, D. T. Borup, S. A. Johnson, and M. Berggren, "Non-linear inverse scattering: High resolution quantitative breast tissue tomography," *J. Acoust. Soc. Am.,* pp. 3802-3813, 2012.

[14] J. Wiskin, D. Borup, and S. Johnson, "Inverse Scattering Theory," in *Acoustical Imaging 30*, ed New York, Dordrecht, Heidelberg, London: Springer, 2011, pp. 54-59.

[15] J. W. Wiskin, D. T. Borup, E. Iuanow, J. Klock, and M. W. Lenox, "3-D Nonlinear Acoustic Inverse Scattering: Algorithm and Quantitative Results," *IEEE Transactions on Ultrasonics, Ferroelectrics, and Frequency Control,* vol. 64, pp. 1161-1174, 2017.

[16] C. Li, N. Duric, P. Littrup, and L. Huang, "In Vivo Breast sound-speed imaging with ultrasound tomography," *Ultrasound. Med. Biol. ,* pp. 1615-1628, 2009.

[17] P. Huthwaite and F. Simonetti, "High-resolution imaging without iteration: A fast and robust method for breast ultrasound tomography," *Journal of the Acoustical Society of America,* vol. 130, pp. 1721-1734, 2011.

[18] L. N. Trefethen and L. Halpern, "Wide-angle one way wave equations," *J. Acoustical Society of America,* vol. 84, pp. 1397-1404, 1988.

[19] F. D. Tappert, "The parabolic equation method," in *Wave propagation and underwater acoustics, Lecture Notes in Physics 70*, ed New York: Springer-Verlag, 1977.

[20] M. Andre, J. Wiskin, D. Borup, S. Johnson, H. Ojeda-Fournier, and L. Olson, "Quantitative volumetric breast imaging with 3D inverse scatter computed tomography," *Conf Proc IEEE Eng Med Biol Soc,* vol. 2012, pp. 1110-3, 2012.

[21] J. Wiskin, B. Malik, R. Natesan, and M. Lenox, "Quantitative assessment of breast density using transmission ultrasound tomography," *Medical Physics,* vol. 46, pp. 2610-2620, 2019.